Available online at www.sciencedirect.com
ScienceDirect
Earth and Planetary Science Letters 254 (2007) 115–126
EPSL
www.elsevier.com/locate/epsl

A FUN-like hibonite inclusion with a large ^{26}Mg-excess

Takayuki Ushikubo [a,*], Hajime Hiyagon [b], Naoji Sugiura [b]

[a] Department of Geology and Geophysics, University of Wisconsin-Madison, 1215 W. Dayton St., Madison, WI 53706, USA
[b] Department of Earth and Planetary Science, The University of Tokyo, 7-3-1. Hongo, Bunkyo, Tokyo, 113-0033, Japan

Received 17 April 2006; received in revised form 16 November 2006; accepted 16 November 2006
Available online 4 January 2007
Editor: R.W. Carlson

Abstract

We found a unique hibonite ($CaAl_{12}O_{19}$) inclusion Kz1–2 from the Kainsaz (CO3) chondrite, which exhibits evidence for a strong link between "normal" CAIs and FUN inclusions. Kz1–2 shows strongly fractionated isotopic compositions of O, Ca, and Ti preferring heavy isotopes and a characteristic REE abundance pattern similar to those of FUN (or HAL-type hibonite) inclusions, suggesting an intensive distillation process in the formation of this inclusion. Unlike FUN inclusions, however, Kz1–2 shows large excesses in ^{26}Mg and possibly in ^{41}K most likely from the decays of now-extinct nuclides ^{26}Al and ^{41}Ca with the inferred initial ratios of $(^{26}Al/^{27}Al)_0 \sim 5.3 \times 10^{-5}$ and $(^{41}Ca/^{40}Ca)_0 \sim 1.1 \times 10^{-8}$, respectively, and no detectable mass-independent isotopic anomalies in Ca and Ti, both of which are characteristic of "normal" CAIs. These observations suggest that the distillation process which produced isotopic fractionation in Kz1–2 occurred as early as the formation of "normal" CAIs. It is also inferred that the formation process of FUN inclusions is closely related to that of "normal" CAIs.

Keywords: FUN inclusion; CAI; isotope; early solar system; short-lived nuclide; hibonite

1. Introduction

Refractory inclusions, also called Ca–Al-rich inclusions or CAIs, are composed mostly of refractory minerals with condensation temperatures >1300 K (e.g. [1,2]) and are considered to have formed at high temperatures. They have the oldest ^{207}Pb/^{206}Pb ages of 4567.2 Ma [3] so far obtained for solar system materials. Early formation of CAIs is also supported by the existence of excesses in ^{26}Mg [4,5] and ^{41}K [6,7], which are decay products of the now-extinct short-lived nuclides ^{26}Al (half-life: 0.72 Myr) and ^{41}Ca (half-life: 0.10 Myr), respectively. The inferred initial ^{26}Al/^{27}Al ratios obtained for many CAIs are $\sim 5 \times 10^{-5}$ (so-called "the canonical value") [5] and those of ^{41}Ca/^{40}Ca obtained in recent work are $\sim 1.4 \times 10^{-8}$ [7].

There is a minor group of CAIs, which can be distinguished from other inclusions solely by their isotopic characteristics. They are called FUN inclusions (e.g. [8–10]), in which "F" stands for "Fractionation", due to their fractionated isotopic compositions of many elements (e.g., O, Mg, Si, Ca, and Ti) preferring heavier isotopes (the F-signature), and "UN" stands for "Unidentified Nuclear effects" such as enrichment or depletion of ^{48}Ca and ^{50}Ti (the UN-signature). Although the F- and UN-signatures are often accompanied with each other, some inclusions have only F- or only UN-signature, and in such

* Corresponding author. Tel.: +1 608 265 2601; fax: +1 608 262 0693.
E-mail addresses: ushi@geology.wisc.edu (T. Ushikubo), hiyagon@eps.s.u-tokyo.ac.jp (H. Hiyagon), sugiura@eps.s.u-tokyo.ac.jp (N. Sugiura).

0012-821X/$ - see front matter © 2006 Elsevier B.V. All rights reserved.
doi:10.1016/j.epsl.2006.11.031

cases, we may call them as F inclusions or UN inclusions, respectively. Most of the CAIs other than F, UN, and FUN inclusions may be called as "normal CAIs". It has been recognized that FUN inclusions generally have only small or negligible excesses in ^{26}Mg (or ^{41}K) due to decay of ^{26}Al (or ^{41}Ca) [5,7,9–15]. This may be interpreted in different ways; FUN inclusions formed *later* than normal CAIs when these nuclides have mostly decayed, or they formed *earlier* than normal CAIs that formed after the injection of radioactive nuclides ^{26}Al and ^{41}Ca possibly from stellar source(s), or it may be explained by heterogeneity in the abundance of short-lived nuclides in the early solar nebula. Here we report a hibonite inclusion that clearly shows both F-signature and excesses in ^{26}Mg and ^{41}K. This suggests that F (and possibly FUN) inclusions formed very early in the solar system history.

2. Experimental

2.1. Samples

An angular-shaped hibonite inclusion, Kz1–2 (~100 μm × 100 μm in size) was found in a thin section of the Kainsaz CO3 chondrite. It consists mostly of hibonite ($CaAl_{12}O_{19}$) in the interior with small (less than a few micrometers) corundum (Al_2O_3) grains on the outer margin and a thin (~5 μm) rim layer of spinel ($MgAl_2O_4$; Fig. 1). Chemical compositions of minerals in Kz1–2 are shown in Table 1. Hibonite of Kz1–2 contains no detectable MgO and TiO_2 (<0.2%) but it contains small amounts of FeO. Fe content tends to increase toward the outside of the inclusion although it is not clear whether this is an intrinsic feature or a later metamorphic one.

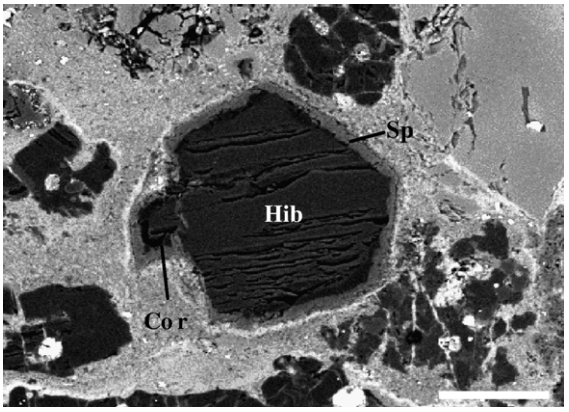

Fig. 1. Backscattered electron image of the hibonite inclusion, Kz1–2. A hibonite crystal (gray) is surrounded by a spinel rim (light gray). Small corundum grains (dark gray) are found between the hibonite crystal and the spinel rim. All phases in Kz1–2 contain significant amounts of FeO (0.3% for hibonite, 0.6% for corundum and 21% for spinel rim). The scale bar is 50 μm.

Table 1
Elemental abundances of Kz1–2

	Hibonite	Spinel	Corundum
MgO	n.d.[a]	13.6	n.d.
Al_2O_3	91.3	61.8	99.4
CaO	8.6	n.d.	n.d.
Cr_2O_3	n.d.	1.0	n.d.
FeO	0.3	21.0	0.6[b]
ZnO	n.d.	0.9	n.d.
Total	100.2	98.2	100.1

[a] n.d. indicates less than detection limit (typically 0.2%).
[b] Fe content of corundum was calculated as Fe_2O_3.

We also found two hibonite-bearing inclusions, Kz1–9 and Kz1–11, on the same thin section. Kz1–11 (~250 μm × 200 μm in size) is an aggregate of blade-shaped hibonite crystals with a thin (<10 μm) diopside rim layer. Kz1–9 (~60 μm in diameter) is a spherule which mostly consists of hibonite and fassaite. Hibonite grains are embedded in fassaite and the whole spherule is surrounded by a thin (<5 μm) diopside rim. Sodium-rich phases (e.g., sodalite) are observed between fassaite and the diopside rim. This inclusion is similar to a hibonite–pyroxene (or hibonite–glass) spherule described previously in [12,16,17].

2.2. Analytical techniques and conditions

Petrographic observation and measurements of the elemental compositions were carried out with a JEOL JMS-5310 scanning electron microscope equipped with a Link-ISIS energy dispersive X-ray analysis system (Oxford Co.) at the University of Tokyo. O, Mg, K, Ca, and Ti isotopes and REE abundances of Kz1–2 were measured with a CAMECA ims-6f ion microprobe at the University of Tokyo. Oxygen isotopic measurements using a Cs^+ primary beam were performed before other measurements (Mg, K, Ca, and Ti isotopes and REE abundances) in order to avoid contamination with the O^- primary beam.

2.2.1. O isotopes

Oxygen isotopes were measured using a 19.5 keV Cs^+ ion beam ~15 μm in diameter with an intensity of ~0.1 nA. Negative secondary ions were accelerated at −9.5 kV and detected with a Faraday Cup (FC, for $^{16}O^-$) or an electron multiplier-based ion counting system (EM, for $^{17}O^-$, $^{16}OH^-$ and $^{18}O^-$). A mass resolving power was set to ~5000 and the contribution of $^{16}OH^-$ signal at the center of the $^{17}O^-$ peak was negligible. A normal incidence electron gun was used for charge compensation.

Repeated analyses were performed on a San Carlos olivine standard ($\delta^{17}O=2.54‰$, $\delta^{18}O=4.92‰$) and all the data of the sample were normalized to the average of data of the San Carlos olivine.

Matrix effects were predetermined for various minerals, but essentially no effects were observed among San Carlos olivine, spinel and pyroxene (both diopside and low Ca pyroxene) within experimental uncertainties (<2‰ for $^{18}O/^{16}O$ ratio). Only corundum and quartz showed large matrix effects; the measured $^{18}O/^{16}O$ ratios for corundum and quartz were 9.5±2.2‰ and 20.9±4.7‰ lower than the true values, respectively, when normalized to the San Carlos olivine data. We do not have hibonite data, but oxygen isotopic compositions measured for coexisting spinel and hibonite in other refractory inclusions usually show no difference within experimental uncertainty (e.g. [18]), suggesting negligible matrix effect for hibonite, too. Hence, we applied no matrix effect corrections in the present analyses for hibonite and fassaite.

2.2.2. ^{26}Al– Mg systematics

Magnesium isotopes and Al/Mg ratios were measured using a 22.5 keV O^- ion beam ~20 μm in diameter with an intensity of ~1.0 nA. Positive secondary ions of Mg and Al were accelerated at +10.0 kV and detected with a Faraday Cup (FC, for $^{27}Al^+$) or an electron multiplier-based ion counting system (EM, for $^{24}Mg^+$, $^{25}Mg^+$ and $^{26}Mg^+$). A mass resolving power was set to about 4500 and the contribution of $^{48}Ca^{2+}$ signal at the center of the $^{24}Mg^+$ peak and that of $^{24}MgH^+$ signal at the center of the $^{25}Mg^+$ peak were negligible.

Deviations of the measured Mg isotopic ratios from the terrestrial values, $^{25}Mg/^{24}Mg=0.12663$ and $^{26}Mg/^{24}Mg=0.13932$ [19], were expressed as follows: $\Delta^{25}Mg=\{(^{25}Mg^+/^{24}Mg^+)/0.12663-1\}\times1000$ and $\Delta^{26}Mg=\{(^{26}Mg^+/^{24}Mg^+)/0.13932-1\}\times1000$ (‰), respectively. Intrinsic mass fractionation of the sample (F(Mg)) was determined by $F(Mg)=\Delta^{25}Mg(sample)-\Delta^{25}Mg(standard)$ (‰/amu), where Madagascar hibonite was used for the terrestrial standard. The mass-independent isotopic anomaly of ^{26}Mg was determined by a linear correction of mass-dependent isotopic fractionation, $\delta^{26}Mg=\Delta^{26}Mg-2\times\Delta^{25}Mg$ (‰). The $^{27}Al/^{24}Mg$ ratio was determined by multiplying the measured $^{27}Al^+/^{24}Mg^+$ ratio by 1.16 (±0.05), a relative sensitivity factor determined by the analysis of Madagascar hibonite standard.

2.2.3. ^{41}Ca– K systematics

Potassium isotopes and Ca/K ratios were measured using a 22.5 keV O^- ion beam ~30 μm in diameter with an intensity of ~3.0 nA. Positive secondary ions of K and Ca were accelerated at +10.0 kV and detected with a Faraday Cup (FC, for $^{40}Ca^+$) or an electron multiplier-based ion counting system (EM, for $^{39}K^+$, $^{41}K^+$, $^{40}Ca^{43}Ca^{2+}$, $^{42}Ca^+$ and $^{43}Ca^+$). Secondary ions emitted from the central ~15 μm area of the beam spot were measured by limiting the ions using a "field aperture" placed on the focal plane of the secondary ion image of the sample surface. A mass resolving power was set to ~6500 and the contribution of $^{40}CaH^+$ signal at the center of the $^{41}K^+$ signal was negligible. Although interferences of $^{84}Sr^{2+}$ and $^{86}Sr^{2+}$ for $^{42}Ca^+$ and $^{43}Ca^+$, respectively, cannot be resolved at this mass resolution, their contributions were negligible judging from the $^{87}Sr^{2+}$ signal.

Corrections that may be needed for accurate ^{41}K measurements are $^{40}Ca^{42}Ca^{2+}$ interference and background noise of the EM. Contribution of the $^{40}Ca^{42}Ca^{2+}$ interference was estimated from $^{42}Ca^+$ multiplied by $^{40}Ca^{43}Ca^{2+}/^{43}Ca^+$, instead of $^{40}Ca^{42}Ca^{2+}/^{42}Ca^+$, a similar method used by Srinivasan et al. [20]. This ratio, $^{40}Ca^{43}Ca^{2+}/^{43}Ca^+$, varies from one mineral to another, as demonstrated by Srinivasan et al. [20]. In this study, the $^{40}Ca^{43}Ca^{2+}/^{43}Ca^+$ ratio was determined by the mean value measured in Kz1–2 (~1.5×10^{-6}). We note that our ratios of $^{40}Ca^{43}Ca^{2+}/^{43}Ca^+$ for hibonite are smaller than that (~7×10^{-6}) used by Srinivasan et al. [20], possibly due to slightly different analytical conditions. The background noise of EM in our system

Table 2
Relative sensitivity factors and mono-oxide production ratios used in the present study

	RSF[a]	RO^+/R^+[b]
Ba	0.56	0.048
La	0.67	0.217
Ce	0.60	0.230
Pr	0.60	0.183
Nd	0.69	0.154
Sm	0.73	0.087
Eu	0.75	0.064
Gd	0.72	0.138
Tb	0.69	0.135
Dy	0.70	0.104
Ho	0.70	0.103
Er	0.62	0.103
Tm	0.66	0.093
Yb	0.55	0.075
Lu	0.50	0.133
Hf	0.24	

[a] Relative sensitivity factor (RSF) compared with Ca^+ intensity: $RSF=(R^+/Ca^+)_{obs}/(R/Ca)_{real}$, where R stands for Ba, REEs or Hf.
[b] Production ratios of mono-oxide ions/atomic ions: R stands for Ba or REEs (nominal values at an energy offset of 60 eV).

was about 0.003 counts/s and was important only for the $^{40}Ca^{43}Ca^{2+}$ measurements. Isotopic ratios were calculated based on the averaged ion counts of the whole data rather than the average of the isotopic ratios obtained for individual measurement cycles. This is because an average of isotopic ratios would give an overestimated value at small count rates; in an extreme case, for example, an isotopic ratio would become infinite when the count of the denominator isotope happens to be zero in one of the measurement cycles.

$^{40}Ca/^{39}K$ ratio was determined by multiplying the measured $^{40}Ca^+/^{39}K^+$ by 3.0(±0.1), a relative sensitivity factor determined for terrestrial feldspar. This value is very close to the previous value of 3.1 determined for terrestrial pyroxene [20].

2.2.4. Ca and Ti isotopes

Ca and Ti isotopes were measured using a 22.5 keV O^- ion beam ~30 μm in diameter with an intensity of ~3.0 nA. Positive secondary ions were accelerated at +10.0 kV and detected with an EM. $^{40}Ca^+$, $^{42}Ca^+$, $^{43}Ca^+$, $^{87}Sr^{2+}$, $^{44}Ca^+$, $^{48}Ca^+$, and $^{48}Ti^+$ were measured for Ca isotopic measurements and $^{48}Ca^+$, $^{46}Ti^+$, $^{47}Ti^+$, $^{48}Ti^+$, $^{49}Ti^+$, $^{50}Ti^+$, $^{51}V^+$, and $^{52}Cr^+$ were measured for Ti isotopic measurements. Secondary ions emitted from the central ~15 μm area of the beam spot were measured using the analytical method for the Ca–K systematics. A mass resolving power was set to ~10,000 to resolve hydride signals and ^{48}Ti from ^{48}Ca.

Since interferences of $^{50}V^+$ and $^{50}Cr^+$ for $^{50}Ti^+$ cannot be resolved at this mass resolution, $^{51}V^+$ and $^{52}Cr^+$ signals were measured to estimate the contributions of $^{50}V^+$ and $^{50}Cr^+$ for $^{50}Ti^+$. Assuming that $^{50}V/^{51}V$ and $^{50}Cr/^{52}Cr$ of the Kz1–2 were equal to the terrestrial value (0.002503 and 0.051859, respectively), the estimated $^{50}V^+$ signal was very small and negligible ($^{50}V^+/^{50}Ti^+ < 0.0001$) but the estimated $^{50}Cr^+$ signal was not negligible and the correction for $^{50}Ti^+$ was about 1%.

Table 3
Isotopic compositions of Kz1–2

Oxygen	$\delta^{17}O$ (‰) [a]		$\delta^{18}O$ (‰) [a]		$\Delta^{17}O$ (‰) [a]	
San Carlos olivine	2.5	±1.5	4.9	±2.0	0.0	±1.2
Kz1–2	−13.7	±1.5	6.1	±2.0	−16.9	±1.3

Magnesium	$^{27}Al/^{24}Mg$		F(Mg) (‰/amu) [a]		$\delta^{26}Mg$ (‰)		$(^{26}Mg/^{24}Mg)$	
Madagascar hibonite	18.5	±1.6	*0.0*	±1.0	0.1	±2.3	0.13934	±0.00031
Kz1–2 hibonite #1	613.0	±54.2	4.7	±3.1	222.5	±8.7	0.17031	±0.00121
Kz1–2 hibonite #2	4789.4	±425.9	−26.6	±29.2	2029.5	±100.1	0.42207	±0.01394

Potassium	$^{40}Ca/^{39}K$		$^{41}K/^{39}K$		$(^{40}Ca^{43}Ca)^{2+}/^{43}Ca^+$	
Madagascar hibonite	4.55e+3	±8.7e+1	0.0719	±0.0006	1.66e−6	±5.0e−7
Fassa diopside #1	1.31e+6	±4.6e+4	0.0714	±0.0117	2.54e−5	±3.5e−6
Fassa diopside #2	1.54e+6	±4.0e+4	0.0707	±0.0098	2.30e−5	±1.0e−6
Fassa diopside #3	2.45e+7	±1.5e+6	0.0307	±0.3142	2.58e−5	±3.0e−6
Kz1–2 hibonite #1	4.55e+5	±2.7e+4	0.0792	±0.0079	1.40e−6	±4.2e−7
Kz1–2 hibonite #2	2.68e+5	±1.3e+4	0.0756	±0.0042	1.40e−6	±4.2e−7
Kz1–2 hibonite #3	2.89e+6	±1.8e+5	0.0780	±0.0274	1.66e−6	±5.0e−7
Kz1–2 hibonite #4	2.54e+5	±1.6e+4	0.0777	±0.0053	1.66e−6	±5.0e−7
Kz1–2 hibonite #5	7.38e+5	±3.8e+4	0.0880	±0.0110	1.66e−6	±5.0e−7

Calcium	α		F(Ca) (‰/amu) [a]		$\delta^{42}Ca$ (‰)		$\delta^{43}Ca$ (‰)		$\delta^{48}Ca$ (‰)	
Madagascar hibonite	−0.12	±0.04	*0.0*	±1.1	−1.4	±3.5	−0.6	±6.7	−1.0	±3.7
Kz1–2 hibonite	0.58	±0.03	16.4	±1.3	−0.4	±4.7	−0.9	±7.3	−1.4	±5.0

Titanium	β		F(Ti) (‰/amu) [a]		$\delta^{47}Ti$ (‰)		$\delta^{49}Ti$ (‰)		$\delta^{50}Ti$ (‰)	
Madagascar hibonite	−0.69	±0.19	*0.0*	±4.2	1.5	±1.4	1.2	±1.5	0.2	±1.9
Kz1–2 hibonite	−0.19	±0.26	10.9	±7.0	7.9	±11.5	−6.6	±11.7	−7.3	±14.8

Errors of O isotopes are 1σ and errors of other isotopes are 2σ.
[a] Data of sample are normalized to those of terrestrial minerals.

The contributions of $^{84}Sr^{2+}$ and $^{86}Sr^{2+}$ signals for $^{42}Ca^{+}$ and $^{43}Ca^{+}$ signals were negligible.

After corrections of interferences, the observed Ca and Ti isotopic ratios were normalized to the terrestrial values of Ca and Ti [21,22]. The intrinsic mass fractionation of Ca and Ti isotopes of the sample, F(Ca) and F(Ti), respectively, were determined by $F(Ca)=\Delta^{40}Ca$(the sample) $-\Delta^{40}Ca$(Madagascar hibonite) and $F(Ti)=\Delta^{46}Ti$(the sample) $-\Delta^{46}Ti$(Madagascar hibonite) (‰/amu), where $\Delta^{40}Ca=-\{(^{40}Ca^{+}/^{44}Ca^{+})/47.153-1\}\times 1000/4$ and $\Delta^{46}Ti=-\{(^{46}Ti^{+}/^{48}Ti^{+})/0.108548-1\}\times 1000/2$. The mass-independent isotopic anomalies of ^{i}Ca and ^{j}Ti were calculated according to the exponential isotopic mass fractionation law [23]:

$$\delta^{i}\mathrm{Ca}=\left(\frac{\left(^{i}\mathrm{Ca}^{+}/^{44}\mathrm{Ca}^{+}\right)_{\mathrm{measured}}\times(m_i/44)^{-\alpha}}{\left(^{i}\mathrm{Ca}^{+}/^{44}\mathrm{Ca}^{+}\right)_{\mathrm{literature}}}-1\right)\times 1000$$

$$\delta^{j}\mathrm{Ti}=\left(\frac{\left(^{j}\mathrm{Ti}^{+}/^{48}\mathrm{Ti}^{+}\right)_{\mathrm{measured}}\times(m_j/48)^{-\beta}}{\left(^{j}\mathrm{Ti}^{+}/^{48}\mathrm{Ti}^{+}\right)_{\mathrm{literature}}}-1\right)\times 1000\quad(‰)$$

where α and β were determined by $(^{40}Ca^{+}/^{44}Ca^{+})_{sample}/47.153=(40/44)^{\alpha}$ and $(^{46}Ti^{+}/^{48}Ti^{+})_{sample}/0.108548=(46/48)^{\beta}$.

2.2.5. Rare earth elements

REE abundances were measured using a 22.5 keV O^{-} ion beam ~20 μm in diameter with an intensity of ~1.0 nA. Positive secondary ions were accelerated at +10.0 kV and signals from 133 amu to 185 amu, which correspond to ions of Ba^{+} to Hf^{+}, were detected by an EM. A mass resolving power was set to ~300 to obtain maximum intensities of secondary ions. An energy filtering method, with an energy offset of 60 V and an energy window of 30 V, was applied for the REE analyses to reduce the effects of complex molecular interferences. Because of the low mass resolving power, atomic (M^{+}) and oxide (MO^{+}) ion signals were not resolved (e.g. $^{156}Gd^{+}$ and $^{140}Ce^{16}O^{+}$ were observed at 156 amu), where M represents Ba, REE, and Hf. Hence, the observed signals of masses 135 to 184 amu were mathematically deconvolved into atomic (M^{+}) and oxide (MO^{+}) ion signals using a method slightly modified from that described in [24]. Also some major element ions such as $^{40}Ca^{+}$, $^{24}Mg^{+}$, $^{27}Al^{+}$ and $^{28}Si^{+}$ were analyzed with a Faraday Cup. Absolute abundances of Ba, REE, and Hf were determined by the observed M^{+}/Ca^{+} ratios and predetermined relative sensitivity factors, $(M^{+}/Ca^{+})_{\text{ion probe}}/(M/Ca)_{true}$, and Ca concentration in the analyzed spots determined after the ion microprobe analyses. Oxide production ratios (MO^{+}/M^{+}) and sensitivity factors of M^{+} relative to Ca^{+} were predetermined using synthetic glass standards and NIST 612 standard (Table 2) and used for the calculation. The former were mainly used for determination of oxide production ratios and the latter for determination of relative sensitivity factors.

3. Results

The results of the isotopic measurements are summarized in Table 3. Oxygen isotopic compositions of Kz1–2 and other two hibonite-bearing inclusions, Kz1–9 and Kz1–11, are illustrated in Fig. 2. For comparison, O isotopic compositions of three HAL-type hibonite inclusions, HAL, 7-404, and 7-971, previously reported in [11,25] are also shown. In contrast to Kz1–9 and Kz1–11, O isotopic composition of Kz1–2 is located to the right of the CCAM line like those of HAL-type hibonite inclusions. This is characteristic of FUN inclusions. It is considered that precursors of the FUN inclusions originally had $\delta^{17}O\sim\delta^{18}O\sim-50‰$ like common refractory inclusions and that mass-dependent fractionation caused by an intense distillation process and late

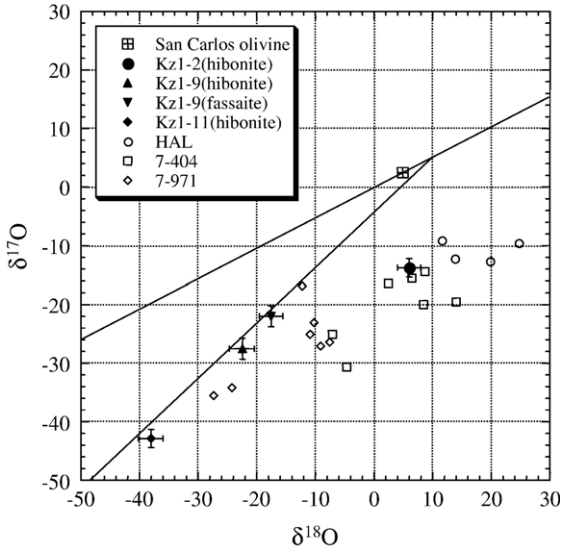

Fig. 2. Oxygen isotopic compositions of Kz1–2 (large filled circle) and other hibonite-bearing inclusions, which were found in the same thin section (small filled symbols). Errors are 1σ. Oxygen isotopic compositions of HAL-type hibonite inclusions (open symbols) are also shown [11,25]. The terrestrial fractionation line and the Carbonaceous Chondrite Anhydrous Minerals line are shown for reference. In contrast to O isotopic compositions of other hibonite-bearing inclusions on the same thin section, that of Kz1–2 is located to the right of the CCAM line, which is a characteristic of HAL-type hibonite inclusions. The oxygen isotopic composition of Kz1–2 can be explained by a mass fractionation and a mixing with the solar nebular gas.

mixing with normal O (located somewhere near the TF line) produced the characteristic O isotopic compositions of FUN inclusions [8,25,26]. The oxygen isotopic composition of Kz1–2 suggests that this inclusion also experienced an intense distillation process.

Fig. 3 shows the results of Mg and K isotopic measurements of Kz1–2. This inclusion has extremely large positive anomaly in ^{26}Mg (up to ~+2030‰) and the inferred initial ^{26}Al/^{27}Al ratio is $(5.33\pm0.16)\times10^{-5}$, assuming that δ^{26}Mg is 0‰ for ^{27}Al/^{24}Mg=0 (Fig. 3a).

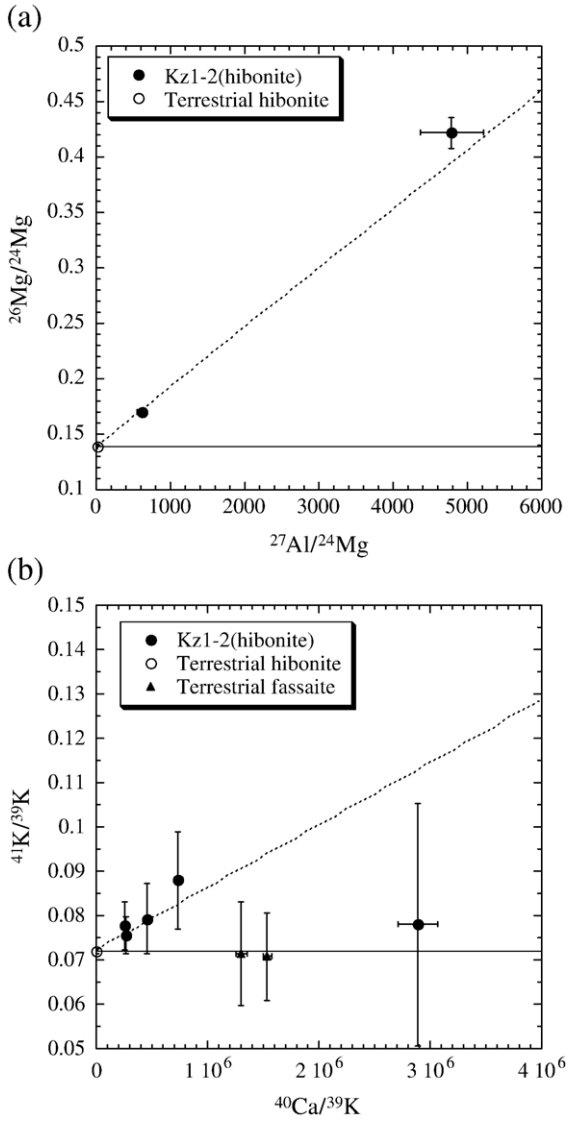

Fig. 3. (a) Al–Mg plot for Kz1–2. The broken line is the best fit line assuming the initial ^{26}Mg/^{24}Mg=0.13932 (the terrestrial value, solid line). The inferred initial ^{26}Al/^{27}Al is $(5.33\pm0.16)\times10^{-5}$ (broken line). (b) Ca–K plot for Kz1–2. All ^{41}K/^{39}K data tend to show higher than the terrestrial value of 0.072 (solid line). The inferred ^{41}Ca/^{40}Ca=1.4×10^{-8} obtained by Sahijpal et al. [7] is shown by the broken line. Errors are 2σ.

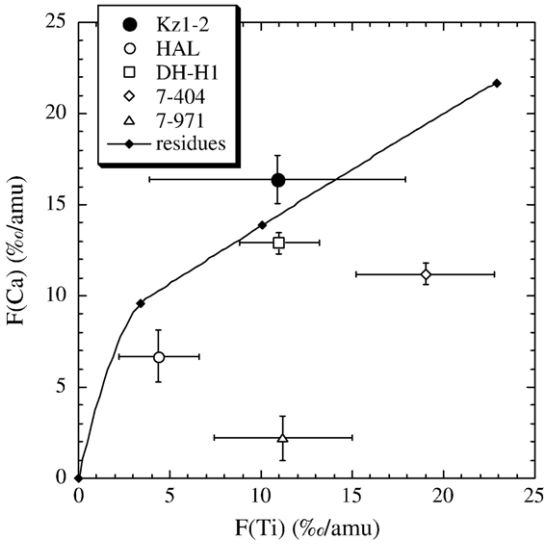

Fig. 4. Mass-dependent isotopic fractionation of Ca, F(Ca), and Ti, F (Ti) of Kz1–2 and other HAL-type hibonite inclusions [11,23]. Those of residue of the evaporation experiment in vacuum that was performed by Floss et al. [30] are also shown. Among five HAL-type hibonite inclusions, 7-404 and 7-971 have heavier Ti isotopes than the isotopic evolution curve of residues. Errors are 2σ.

This is close to ^{26}Al/^{27}Al ~ 5×10^{-5}, which is commonly observed in normal CAIs [5], and ^{26}Al/^{27}Al ~ 5.9×10^{-5}, which is recently obtained by isochrones comprised of bulk CAIs [27–29]. Five measurements were performed for K isotopes and the results tend to show positive ^{41}K isotopic anomalies though clear excess ^{41}K beyond 2σ error is observed only for one datum. Although the correlation in Fig. 3b is not good, we may calculate the initial ^{41}Ca/^{40}Ca ratio from the present results. Assuming that excess in ^{41}K was derived from a decay of ^{41}Ca and

Table 4
CI normalized REE abundances of Kz1–2

	Hibonite	
La	69.7	±7.7
Ce	0.1	<
Pr	46.1	±6.2
Nd	41.8	±4.8
(Pm)		
Sm	27.0	±3.9
Eu	14.1	±11.0
Gd	17.9	±2.9
Tb	10.5	±3.8
Dy	14.4	±2.1
Ho	27.2	±4.6
Er	39.9	±4.9
Tm	33.1	±6.2
Yb	1.6	±0.9
Lu	40.9	±8.3

Errors are 2σ.

the initial $^{41}K/^{39}K$ ratio is 0.0722 for $^{40}Ca/^{39}K=0$, we obtain the inferred initial $^{41}Ca/^{40}Ca$ ratio to be $(1.07\pm0.63)\times10^{-8}$, which is close to those of common refractory inclusions ($^{41}Ca/^{40}Ca\sim1.4\times10^{-8}$ [7]).

Ca and Ti isotopes of Kz1–2 show strong positive fractionation with F(Ca)=16.4±1.3‰/amu and F(Ti)=10.9±7.0‰/amu (Table 3). Fig. 4 shows F(Ca), and F(Ti) of Kz1–2 and those of other HAL-type hibonite inclusions [11,23]. Those of evaporation residues that were studied by Floss et al. [30] were also shown in Fig. 4. Kz1–2 shows higher F(Ca) than but comparable F(Ti) to those of other HAL-type hibonite inclusions. No clear correlation is found between F(Ca) and F(Ti) among all these inclusions (Fig. 4). Kz1–2 does not show clear excesses or depletions in ^{48}Ca and ^{50}Ti within analytical errors (~5‰ for $\delta^{48}Ca$ and ~15‰ for $\delta^{50}Ti$; Table 3). Because of low concentration of Ti in Kz1–2 (less than 0.2% in TiO_2) and the count rate of a $^{50}Ti^+$ signal was one order of magnitude less than that of a $^{48}Ca^+$ signal, errors of Ti isotopic measurements are large.

Kz1–2 has characteristic fractionated REE abundances (Table 4 and Fig. 5). Firstly, abundances of Ce (<0.1×CI) and Yb (~1×CI) are significantly lower than those of other REEs (from ~10×CI to ~70×CI). Secondly, abundances of LREE tend to decrease but those of HREE tend to increase with decreasing ionic radius, resulting in a concave REE pattern. Such a pattern is similar to those for the other HAL-type hibonite inclusions [12,31,32] (Fig. 5). Two typical REE patterns can be identified in the HAL-type hibonite inclusions. One type shows gradual decrease in abundance from La to Yb with a large depletion in Ce and a small enrichment in Lu (HAL and DH-H1). The other type shows a concave REE pattern with significant depletions in Ce, Eu, and Yb (7-404, 7-971, and Isna SP16). Kz1–2 seems to have an intermediate REE pattern of these two.

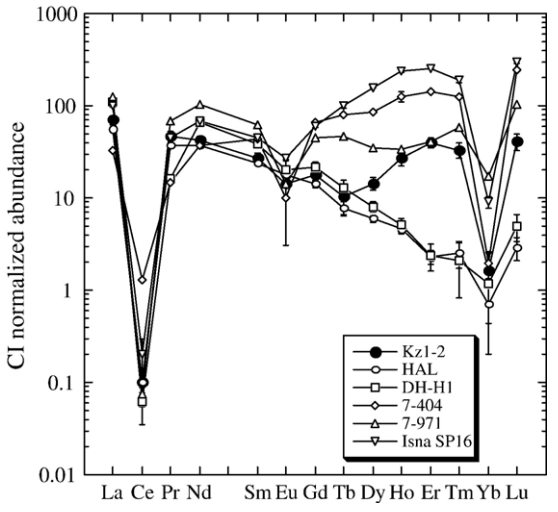

Fig. 5. REE abundances of Kz1–2 and other HAL-type hibonite inclusions [12,31,32]. All of them have a large negative anomaly in Ce, which is probably caused by evaporative loss of Ce when they formed. HREE fractionation pattern of Kz1–2 shows an intermediate pattern between roll-off (HAL and DH-H1) and HREE-enrichment (7-404, 7-971, and Isna SP16). Errors are 2σ.

4. Discussions

4.1. The formation process of Kz1–2 and its timing

Positively fractionated isotopic compositions in O, Ca, and Ti (the F-signature) and the characteristic REE pattern of Kz1–2 suggest that this inclusion is closely related to HAL-type hibonite inclusions. Kz1–2, however, has large ^{26}Mg and ^{41}K excesses but no significant mass-independent isotopic anomalies in ^{48}Ca and ^{50}Ti (the UN-signature). These signatures are common with normal CAIs.

It should be noted that the F-signature and the UN-signatures have independent information, though they are frequently observed together in the same inclusion. The former reflects a physical condition which caused a distillation event, while the latter reflects isotopic signatures of the precursor material. In fact, isotopic anomalies in ^{48}Ca and ^{50}Ti of some hibonite-bearing UN inclusions (without an F-signature) are much larger than those for FUN inclusions (with an F-signature) [12,16,17,23,33–39]. Hence, we consider the F- and UN-signatures separately to understand the origin of F, UN and FUN inclusions as well as normal CAIs.

Positively fractionated isotopic compositions in O, Ca and Ti (Figs. 2 and 4) suggest that Kz1–2 experienced severe distillation while this inclusion was molten [30,40,41]. In contrast, compact-type CAIs usually show only small or no isotopic fractionations although they have evidence for crystallization from once molten droplets. These suggest that FUN inclusions formed in more tenuous nebular gas environment or less dust enriched environment than those of normal CAIs and that equilibration between melt and the surrounding (once evaporated) gas was extremely restricted [e.g. [42]].

The extremely low MgO content of hibonite in Kz1–2 is also consistent with intense distillation. It is not surprising, however, that we cannot detect any fractionated Mg remaining in Kz1–2 because Mg must have been almost completely evaporated from the precursor during the distillation event where even Ca and Ti were

largely evaporated. For the same reason, it is not likely that a detectable amount of fractionated K, which is much more volatile than Mg, remained in Kz1–2. Hence, we consider that possible excess ^{41}K observed in Kz1–2 (Fig. 3b) is most likely due to *in situ* decay of ^{41}Ca.

Ca and Ti isotopic fractionations (F(Ca) and F(Ti), respectively) in Kz1–2 and other HAL-type hibonite inclusions do not correlate well (Fig. 4). Although F(Ca) and F(Ti) data of HAL, DH-H1, and Kz1–2 are plotted along the isotopic evolution curve of evaporation residues from the bulk Allende composition [30], those of 7-404 and 7-971 data are deviated from the isotopic evolution curve and show heavier Ti isotopes. Because it is difficult to suppress Ca isotope fractionation alone, this may suggest that HAL-type hibonite inclusions were formed from different initial compositions of the precursor materials.

The large negative Ce anomaly observed in the REE pattern of Kz1–2 (Fig. 5) indicates that this inclusion was formed under an oxidizing condition because Ce becomes more volatile than other REEs under oxidizing conditions [31,43]. It has been experimentally demonstrated that a large Ce depletion can be produced when a melt is evaporated under a high vacuum [11,30,41,44]. In contrast, no Ce depletion was caused by evaporation experiments under reducing conditions [45]. Because a Ce depletion is characteristic of HAL-type hibonite inclusions that have positively fractionated isotopes, intensive distillation processes and oxidizing conditions could be closely related (e.g., the occurrence of intensive heating in a dust-enriched region or in the absence of a reducing hydrogen-rich nebular gas).

The characteristic concave REE pattern in Kz1–2 has also been observed in some other HAL-type hibonite inclusions (Fig. 5). This REE pattern seems a mixture of two effects: 1) a gradual decrease in REE abundance that is caused by partitioning when hibonite crystallized [46] and 2) an enrichment of HREE. Enrichment of Tm comparable to those of Er and Lu suggests that HREE enrichment was caused under an oxidizing condition [43]. If the distillation processes that formed some HAL-type hibonite inclusions were so intense to cause HREE enrichment compared with LREE, the concave REE pattern could be explained consistently. In this case, it is required that a phase that partitioned REE with hibonite. However, Kz1–2 consists of hibonite, spinel, and corundum and we could not identify any appropriate phase. A tiny phase or glass that partitioned REE with hibonite may be preserved in Kz1–2. The positively fractionated isotopic compositions and characteristic REE fractionation of Kz1–2 strongly suggest that this inclusion formed through an intense distillation process which is similar to those of other HAL-type hibonite inclusions.

On the other hand, Kz1–2 has high abundance of excess ^{26}Mg and a hint of excess ^{41}K with the inferred initial ratios of $(5.33\pm0.16)\times10^{-5}$ for ^{26}Al/^{27}Al and $(1.07\pm0.63)\times10^{-8}$ for ^{41}Ca/^{40}Ca, respectively, although the latter value is rather uncertain. These values are comparable to those of normal CAIs: ^{26}Al/^{27}Al = 5 to 6×10^{-5} [5,27–29] and ^{41}Ca/^{40}Ca $\sim1.4\times10^{-8}$ [7], respectively. As noted previously, the F-signature in Kz1–2 was most likely produced through intense distillation from a molten precursor. Any excesses in ^{26}Mg or ^{41}K produced prior to this high temperature event would be completely erased during the molten stage by mixing with abundant normal Mg and K isotopes. Hence, the fact that Kz1–2 has a large excess in ^{26}Mg (and a possible excess in ^{41}K) corresponding to ^{26}Al/^{27}Al of normal CAIs suggests that the time of the distillation event experienced by Kz1–2 is as early as the formation of normal CAIs. Caillet et al. [47] reported that a unique wollastonite-bearing CAI, White Angel, has both a large mass-dependent fractionation in Mg (~15‰/amu on average in the interior of the inclusion) and a high inferred ^{26}Al/^{27}Al ratio of $(5.3\pm0.6)\times10^{-5}$. This also suggests a possibility of an early occurrence of the distillation event. The relationship between White Angel and FUN inclusions, however, is not clear because this inclusion has unusual wollastonite-rich texture and the Group II REE pattern, which indicates more complicated formation process(es) of White Angel. In this sense, the similarity in the texture and the F-signature of Kz1–2 and those of HAL-type hibonite inclusions is remarkable.

The fact that Kz1–2 has the F-signature, no UN-signature and high initial abundance(s) of ^{26}Al (and ^{41}Ca) suggests that: (1) Kz1–2 has experienced an intensive distillation process similar to those for FUN and HAL-type hibonite inclusions; (2) the precursor material of Kz1–2 is common with those of normal (non-FUN) CAIs with canonical ^{26}Al (and ^{41}Ca) abundance(s); and (3) the formation of Kz1–2 (the timing of the distillation event) is as early as the formation of normal CAIs. Hence, Kz1–2 has strong links both to normal CAIs and to FUN and HAL-type hibonite inclusions. This may suggest that the formation process of FUN inclusions is closely related to those of normal CAIs and that FUN inclusions formed as early as normal CAIs.

4.2. Implications for the isotopic heterogeneity in the early solar nebula

The oxygen isotopic compositions of UN inclusions (mostly hibonite-bearing inclusions) are ^{16}O-rich with

$\delta^{17}O \sim \delta^{18}O \sim -40‰$ to $-50‰$, similar to those of normal CAIs [48–52]. The precursor materials of FUN and F inclusions, including the present hibonite inclusion Kz1–2, also seem to share the same ^{16}O-rich composition before the large mass-dependent isotopic fractionation event(s) [8,11,53]. This suggests that both UN (including FUN) and normal (including F) inclusions formed in an ^{16}O-rich environment.

However, the former has variable mass-independent isotopic anomalies in Ca and Ti (UN-signatures) but the latter has mostly homogeneous isotopes. This may be interpreted in terms of isotopic homogenization process of refractory elements in the early solar nebula, i.e., UN inclusions may have formed while isotopic heterogeneity still existed in these refractory elements and normal CAIs may have formed after homogenization of Ca and Ti isotopes. Existence of both positive and negative anomalies in ^{48}Ca and ^{50}Ti relative to the average (solar) isotopic compositions seems consistent with this idea. Note that homogenization of Ca and Ti isotopes among different grains requires extremely high temperatures, where sufficient partial pressures of Ca and Ti exist in the gas phase, but homogenization of O isotopes can proceed at much lower temperatures.

Aluminum is also highly refractory, and in this sense, homogenization of Al isotopes ($^{26}Al/^{27}Al$ ratios) may be considered in a similar way as homogenization of Ca and Ti isotopes. Rather homogeneous initial $^{26}Al/^{27}Al$ ratios of normal CAIs (i.e., 5 to 6×10^{-5}) could be the result of such a homogenization process. However, the situation is not so straightforward. If the canonical $^{26}Al/^{27}Al$ ratio is the result of the isotopic homogenization process, we would expect both super-canonical and sub-canonical ratios for the earlier inclusions formed before isotopic homogenization of Al and other refractory elements (e.g., Ca and Ti), represented by UN and FUN inclusions. However, this is not the case. Inclusions having significant isotopic anomalies (e.g., $|\delta^{50}Ti| > 10‰$) always show very low initial $^{26}Al/^{27}Al$ (and $^{41}Ca/^{40}Ca$) ratios (e.g., [5,37,54]) and super-canonical ratios have never been reported in UN and FUN inclusions. In contrast, inclusions having high (canonical) initial $^{26}Al/^{27}Al$ (and $^{41}Ca/^{40}Ca$) ratios always show no or small Ca and Ti isotopic anomalies (typically less than 10‰ in ^{48}Ca and ^{50}Ti; e.g. [37]). Although uncertainties of $\delta^{48}Ca$ and $\delta^{50}Ti$ in Kz1–2 are still large ($-1.4\pm5.0‰$ and $-7.3\pm14.8‰$, respectively), it is evident that Kz1–2 does not have an isotopic anomaly of larger than 10‰ in ^{48}Ca, which is typically observed in inclusions that show low initial $^{26}Al/^{27}Al$ ratios. It is also expected that Kz1–2 does not have a large isotopic anomaly in ^{50}Ti because isotopic anomalies of ^{48}Ca and ^{50}Ti are usually associated with each other [37]. So, even if we include the present results of Kz1–2, an exclusive correlation between the UN signature and the occurrence of ^{26}Al (and ^{41}Ca) is true. This strongly suggests that abundance(s) of ^{26}Al (and ^{41}Ca) was (were) very low when UN and FUN inclusions formed.

Later formation of UN and FUN inclusions after the decay of ^{26}Al seems unlikely because it is difficult to retain large isotopic anomalies for several million years after the formation of normal CAIs whose isotopes already had been well homogenized. It also seems inconsistent with the present results that Kz1–2, an F-inclusion closely related to FUN and HAL-type hibonite inclusions, formed as early as normal CAIs. Hence, ^{26}Al (and ^{41}Ca) must be introduced (or produced) at some time after the formation of UN and FUN inclusions and before (or during) the formation of normal CAIs.

Two possible models have been proposed. One is that short-lived nuclides were synthesized by irradiation of protostellar cosmic rays near the central proto-Sun [55,56]. The other is that short-lived nuclides except for ^{10}Be were injected from other stellar source when the solar system formed (e.g. [57]).

Lee et al. [56] proposed that the precursors of normal CAIs were derived from the innermost part of the disk (i.e., inside of the reconnection ring; see Fig. 2 in [56]) but the precursors of UN and FUN inclusions were derived from outside of the reconnection ring. Because of the high temperatures and the high flux of energetic particles at the inside of the reconnection ring, isotopes of refractory elements were homogenized and short-lived nuclides were synthesized. In contrast, outside the reconnection ring, isotopic heterogeneity of refractory elements remained and short-lived nuclides were not synthesized as much as those at the inside of the reconnection ring because the temperature was not high enough to homogenize isotopic compositions of refractory elements and materials were not strongly irradiated. This is consistent with the exclusive correlation between the UN signature and the occurrence of ^{26}Al (and ^{41}Ca).

However, this model is inconsistent with the fact that evidence for existence of live ^{10}Be was observed in FUN and UN inclusions [58–61]. Beryllium-10 cannot be produced in stellar sources but is produced by irradiation of (solar) energetic particles. Hence, the decoupled occurrence of ^{10}Be vs. ^{26}Al and ^{41}Ca strongly suggests that energetic particle irradiation is not the primary source of ^{26}Al and ^{41}Ca present in some early solar system solids.

We prefer, therefore, a stellar origin for ^{26}Al and other (not all, e.g., ^{10}Be) short-lived nuclides, which might be introduced at some stage of the early solar system

evolution (e.g., [57]). In this model, UN and FUN inclusions are considered to have formed prior to the injection of ^{26}Al from a stellar source, possibly a supernova or an AGB star. The existence of the UN-signature in UN and FUN inclusions might be the result of incomplete isotopic homogenization at this very early stage of solar system evolution. Normal CAIs might have formed after the injection of ^{26}Al and after homogenization of isotopes of refractory elements (Al, Ca and Ti). This explains rather uniform abundance of ^{26}Al (the canonical value) and the absence of the isotopic anomalies in Ca and Ti (UN-signature) in normal CAIs. The fact that the F-signature is often accompanied with the UN-signature may indicate that intensive distillation events were very active in the earliest stage of the solar system evolution when isotopic heterogeneity still existed in refractory elements (Ca and Ti), though the mechanisms of such distillation events are not clear at present. The present hibonite inclusion Kz1–2 seems to be a rare inclusion, which shows both an F-signature and a high (~canonical) abundance of ^{26}Al (and possible presence of ^{41}Ca), suggesting strong links both to the normal CAIs and to FUN and HAL-type inclusions. This inclusion possibly formed at the earliest time of the formation period of normal CAIs, when injection of ^{26}Al and isotopic homogenization of refractory elements had been completed but intensive distillation events were still active.

5. Conclusions

We found a unique hibonite inclusion Kz1–2 from the Kainsaz (CO3) chondrite, which shows (1) significant mass-dependent isotopic fractionations in O, Ca and Ti (F-signatures), (2) no significant isotopic anomalies in ^{48}Ca and ^{50}Ti (no UN-signatures) and (3) a significant excess in ^{26}Mg and a possible excess in ^{41}K, most likely from the decays of now-extinct short-lived nuclides ^{26}Al and ^{41}Ca with the inferred initial ratios of $^{26}Al/^{27}Al = (5.33 \pm 0.16) \times 10^{-5}$ and $^{41}Ca/^{40}Ca = (1.07 \pm 0.63) \times 10^{-8}$, respectively. The F-signature and the fractionated REE pattern with a large Ce depletion indicate a close relation between Kz1–2 and HAL-type hibonite inclusions, suggesting both of them have experienced intensive distillation. In contrast to HAL-type hibonite inclusions, however, Kz1–2 shows high initial abundance(s) of ^{26}Al (and ^{41}Ca) and no UN-signature, suggesting that Kz1–2 formed from a precursor material similar to those of normal CAIs and that Kz1–2 formed as early as normal CAIs. Hence, Kz1–2 has strong links both to FUN or HAL-type hibonite inclusions and to normal CAIs.

The present results seem to exclude a late formation of UN and FUN inclusions after significant decay of ^{26}Al, but support an earlier formation of UN and FUN inclusions when isotopic heterogeneity still existed in refractory elements. Aluminum-26 (and some other now-extinct short-lived nuclides) must have been introduced (or produced) at some time after the formation of UN and FUN inclusions. Normal CAIs, on the other hand, might form after injection (or production) of ^{26}Al and after homogenization of isotopic compositions of refractory elements. The present results suggest that the intensive distillation process, which formed the F-signature, apparently occurred while normal CAIs formed and that such a process was not restricted to a specific isotopic reservoir (with UN-signatures). The hibonite inclusion Kz1–2 would provide an important example showing close relationships among F-, UN-, FUN-inclusions and normal CAIs.

Acknowledgements

We are very grateful to Dr. A. M. Davis and Dr. K. D. McKeegan for detailed reviews that significantly improved the paper.

References

[1] S. Yoneda, L. Grossman, Condensation of CaO–MgO–Al_2O_3–SiO_2 liquids from cosmic gases, Geochim. Cosmochim. Acta 59 (1995) 3413–3444.
[2] D. Ebel, L. Grossman, Condensation in dust-enriched systems, Geochim. Cosmochim. Acta 64 (2000) 339–366.
[3] Y. Amelin, A.N. Krot, I.D. Hucheon, A.A. Ulyanov, Lead isotopic ages of chondrules and calcium–aluminum-rich inclusions, Science 297 (2002) 1678–1683.
[4] T. Lee, D.A. Papanastassiou, G.J. Wasserburg, Aluminum-26 in the early solar system: fossil or fuel? Astrophys. J. 211 (1977) L107–L110.
[5] G.J. MacPherson, A.M. Davis, E.K. Zinner, The distribution of aluminum-26 in the early solar system—a reappraisal, Meteoritics 30 (1995) 365–386.
[6] G. Srinivasan, A.A. Ulyanov, J.N. Goswami, ^{41}Ca in the early solar system, Astrophys. J. 431 (1994) L67–L70.
[7] S. Sahijpal, J.N. Goswami, A.M. Davis, L. Grossman, R.S. Lewis, A stellar origin for the short-lived nuclides in the early solar system, Nature 391 (1998) 559–561.
[8] R.N. Clayton, T.K. Mayeda, Correlated oxygen and magnesium isotope anomalies in Allende inclusions: I. Oxygen, Geophys. Res. Lett. 4 (1977) 295–298.
[9] G.J. Wasserburg, T. Lee, D.A. Papanastassiou, Correlated O and Mg isotopic anomalies in Allende inclusions: II. Magnesium, Geophys. Res. Lett. 4 (1977) 299–302.
[10] T. Lee, W.A. Russel, G.J. Wasserburg, Calcium isotopic anomalies and the lack of aluminum-26 in an unusual Allende inclusion, Astrophys. J. 228 (1979) L93–L98.
[11] T.R. Ireland, E.K. Zinner, A.J. Fahey, T.M. Esat, Evidence for distillation in the formation of HAL and related hibonite inclusions, Geochim. Cosmochim. Acta 56 (1992) 2503–2520.

[12] S.S. Russell, G.R. Huss, A.J. Fahey, R.C. Greemwood, R. Hutchison, G.J. Wasserburg, An isotopic and petrologic study of calcium–aluminum-rich inclusions from CO3 meteorites, Geochim. Cosmochim. Acta 62 (1998) 689–714.
[13] R.W. Hinton, A. Bishoff, Ion microprobe magnesium isotope analysis of plagioclase and hibonite from ordinary chondrites, Nature 308 (1984) 169–172.
[14] J.C. Huneke, J.T. Armstrong, G.J. Wasserburg, FUN with PANURGE: high mass resolution ion microprobe measurements of Mg in Allende inclusions, Geochim. Cosmochim. Acta 47 (1983) 1635–1650.
[15] G. Srinivasan, G.R. Huss, G.J. Wasserburg, A petrographic, chemical, and isotopic study of calcium–aluminum-rich inclusions and aluminum-rich chondrules from the Axtell (CV3) chondrite, Meteorit. Planet. Sci. 35 (2000) 1333–1354.
[16] T.R. Ireland, Correlated morphological, chemical, and isotopic characteristics of hibonites from the Murchison carbonaceous chondrite, Geochim. Cosmochim. Acta 52 (1988) 2827–2839.
[17] T.R. Ireland, A.J. Fahey, E.K. Zinner, Hibonite-bearing microspherules: a new type of refractory inclusions with large isotopic anomalies, Geochim. Cosmochim. Acta 55 (1991) 367–379.
[18] H. Hiyagon, Highly heterogeneous distribution of oxygen isotopes in a grossite-bearing inclusion from Yamato 81020 (CO3) chondrite, Meteorit. Planet. Sci. 35 (2000) A75 (abstract).
[19] E.J. Catanzaro, T.J. Murphy, E.L. Garner, W.R. Shields, absolute isotopic abundance ratios and atomic weights of magnesium, J. Res. Natl. Bur. Stand. 70a (1966) 453–458.
[20] G. Srinivasan, S. Sahijpal, A.A. Ulyanov, J.N. Goswami, Ion microprobe studies of Efremovka CAIs: II. Potassium isotope composition and ^{41}Ca in the early solar system, Geochim. Cosmochim. Acta 60 (1996) 1823–1835.
[21] F.R. Niederer, D.A. Papanastassiou, Ca isotopes in refractory inclusions, Geochim. Cosmochim. Acta 48 (1984) 1279–1293.
[22] F.R. Niederer, D.A. Papanastassiou, G.J. Wasserburg, The isotopic composition of titanium in the Allende and Leoville meteorites, Geochim. Cosmochim. Acta 45 (1981) 1017–1031.
[23] A.J. Fahey, J.N. Goswami, K.D. McKeegan, E. Zinner, ^{26}Al, ^{244}Pu, ^{50}Ti, REE, and trace element abundances in hibonite grains from CM and CV meteorites, Geochim. Cosmochim. Acta 51 (1987) 329–350.
[24] A.J. Fahey, Ion microprobe measurements of Mg, Ca, Ti and Fe isotopic ratios and trace element abundances in hibonite-bearing inclusions from primitive meteorites. PhD Thesis, Washington University (1988).
[25] T. Lee, T.K. Mayeda, R.N. Clayton, Oxygen isotopic anomalies in Allende inclusion HAL, Geophys. Res. Lett. 7 (1980) 493–496.
[26] A.M. Davis, K.D. McKeegan, G.J. MacPherson, Oxygen-isotopic compositions of individual minerals from the FUN inclusion Vigarano 1623-5, Meteorit. Planet. Sci. 35 (2000) A47 (abstract).
[27] E.D. Young, J.I. Simon, A. Galy, S.S. Russell, E. Tonui, O. Lovera, Super-canonical ^{26}Al/^{27}Al and the residence time of CAIs in the Solar Protoplanetary Disk, Science 308 (2005) 223–227.
[28] M. Bizzarro, J.A. Baker, H. Haack, Mg isotope evidence for contemporaneous formation of chondrules and refractory inclusions, Nature 431 (2004) 275–278.
[29] M. Bizzarro, J.A. Baker, H. Haack, Corrigendum of Mg isotope evidence for contemporaneous formation of chondrules and refractory inclusions, Nature 435 (2005) 1280.
[30] C. Floss, A. El Goresy, E. Zinner, G. Kransel, W. Rammensee, H. Palme, Elemental and isotopic fractionations produced through evaporation of the Allende CV chondrite: implications for the origin of HAL-type hibonite inclusions, Geochim. Cosmochim. Acta 60 (1996) 1975–1997.
[31] R.W. Hinton, A.M. Davis, D.E. Scatena-Wachel, L. Grossman, R.J. Draus, A chemical and isotopic study of hibonite-rich refractory inclusions in primitive meteorites, Geochim. Cosmochim. Acta 52 (1988) 2573–2598.
[32] T.R. Ireland, A.J. Fahey, E. Zinner, Trace-element abundances in hibonites from the Murchison carbonaceous chondrite: constraints on high-temperature processes in the solar nebula, Geochim. Cosmochim. Acta 52 (1988) 2841–2854.
[33] S. Sahijpal, J.N. Goswami, A.M. Davis, K, Mg, Ti and Ca isotopic compositions and refractory trace element abundances in hibonites from CM and CV meteorites: implications for early solar system processes, Geochim. Cosmochim. Acta 64 (2000) 1989–2005.
[34] T.R. Ireland, W. Compston, H.R. Heydegger, Titanium isotopic anomalies in hibonites from the Murchison carbonaceous chondrite, Geochim. Cosmochim. Acta 49 (1985) 1989–1993.
[35] A. Fahey, J.N. Goswami, K.D. McKeegan, E. Zinner, Evidence for extreme ^{50}Ti enrichment in primitive meteorites, Astrophys. J. 296 (1985) L17–L20.
[36] E.K. Zinner, A.J. Fahey, J.N. Goswami, T.R. Ireland, K.D. McKeegan, Large ^{48}Ca anomalies are associated with ^{50}Ti anomalies in Murchison and Murray hibonites, Astrophys. J. 311 (1986) L103–L107.
[37] T.R. Ireland, Presolar isotopic and chemical signatures in hibonite-bearing refractory inclusions from the Murchison carbonaceous chondrite, Geochim. Cosmochim. Acta 54 (1990) 3219–3237.
[38] A.J. Fahey, E. Zinner, G. Kurat, A. Kracher, Hibonite–hercynite inclusion HH-1 from the Lancé (CO3) meteorite: the history of an ultrarefractory CAI, Geochim. Cosmochim. Acta 58 (1994) 4779–4793.
[39] S.B. Simon, A.M. Davis, L. Grossman, E.K. Zinner, Origin of hibonite–pyroxene spherules found in carbonaceous chondrites, Meteorit. Planet. Sci. 33 (1998) 411–424.
[40] A.M. Davis, A. Hashimoto, R.N. Clayton, T.K. Mayeda, Isotopic mass fractionation of Mg_2SiO_4, Nature 347 (1990) 655–658.
[41] A.M. Davis, A. Hashimoto, R.N. Clayton, T.K. Mayeda, Isotopic and chemical fractionation during evaporation of $CaTiO_3$, Lunar Planet. Sci. XXVI (1995) 317–318 (abstract).
[42] C.M.O'D. Alexander, Chemical equilibrium and kinetic constraints for chondrule and CAI formation conditions, Geochim. Cosmochim. Acta 68 (2004) 3946–3969.
[43] A.M. Davis, T. Tanaka, L. Grossman, Chemical composition of HAL, an isotopically-unusual Allende inclusion, Geochim. Cosmochim. Acta 46 (1982) 1627–1651.
[44] J. Wang, A.M. Davis, R.N. Clayton, T.K. Mayeda, A. Hashimoto, Chemical and isotopic fractionation during the evaporation of the FeO–MgO–SiO_2–CaO–Al_2O_3–TiO_2 rare earth element melt system, Geochim. Cosmochim. Acta 65 (2001) 479–494.
[45] A.M. Davis, A. Hashimoto, N. Parsad, Trace element fractionation during evaporation in reducing atmospheres, Lunar Planet. Sci. XXX (1999) (#2023 [CD-ROM]).
[46] A.K. Kennedy, G.E. Lofgren, G.J. Wasserburg, Trace-element partition in coefficients for perovskite and hibonite in meteorite compositions, Chem. Geol. 117 (1994) 379–390.
[47] C. Caillet, E. Zinner, K.D. McKeegan, R.L. Herbig, The White Angel: an enigmatic wollastonite-bearing F inclusion from the Leoville CV3 chondrite, Lunar Planet. Sci. XXVIII (1997) 199–200 (abstract).

[48] R.N. Clayton, N. Onuma, L. Grossman, T.K. Mayeda, Distribution of the pre-solar component in Allende and other carbonaceous chondrites, Earth Planet. Sci. Lett. 34 (1977) 209–224.
[49] J. Aléon, A.N. Krot, K.D. McKeegan, Calcium–aluminum-rich inclusions and amoeboid olivine aggregates from the CR carbonaceous chondrites, Meteorit. Planet. Sci. 37 (2002) 1729–1755.
[50] A.J. Fahey, J.N. Goswami, K.D. McKeegan, E.K. Zinner, ^{16}O excesses in Murchison and Murray hibonites: a case against a late supernova injection origin of isotopic anomalies in O, Mg, Ca, and Ti, Astrophys. J. 323 (1987) L91–L95.
[51] S. Sahijpal, K.D. McKeegan, J.N. Goswami, A.M. Davis, Oxygen isotopic compositions of Murchison hibonites with wide-ranging radiogenic and neutron-rich stable isotope anomalies, Lunar Planet. Sci. XXXII (2000) (#1502 [CD-ROM]).
[52] T. Ushikubo, H. Hiyagon, N. Sugiura, Oxygen, Ca, and Ti isotopic compositions of hibonite-bearing inclusions, Lunar Planet. Sci. XXXVI (2005) (#1283 [CD-ROM]).
[53] A.M. Davis, K.D. McKeegan, G.J. MacPherson, Oxygen-isotopic compositions of individual minerals from the FUN inclusion Vigarano 1623-5, Meteorit. Planet. Sci. 35 (2000) A47 (abstract).
[54] R.N. Clayton, R.W. Hinton, A.M. Davis, Isotopic variations in the rock-forming elements in meteorites, Philos. Trans. R. Soc. Lond., A 325 (1988) 483–501.
[55] M. Gounelle, F.H. Shu, H. Shang, A.E. Glassgold, E.K. Rehm, T. Lee, Extinct radioactivities and protosolar cosmic rays: self-shielding and light elements, Astrophys. J. 548 (2001) 1051–1070.
[56] T. Lee, F.H. Shu, H. Shang, A.E. Glassgold, K.E. Rehm, Protostellar cosmic rays and extinct radioactivities in meteorites, Astrophys. J. 506 (1998) 898–912.
[57] S. Sahijpal, J.N. Goswami, Refractory phases in primitive meteorites devoid of ^{26}Al and ^{41}Ca: representative samples of first solar system solids? Astrophys. J. 509 (1998) L137–L140.
[58] K.K. Marhas, J.N. Goswami, A.M. Davis, Short-lived nuclides in hibonite grains from Murchison: evidence for solar system evolution, Science 298 (2002) 2182–2185.
[59] G.J. MacPherson, G.R. Huss, A.M. Davis, Extinct ^{10}Be in type A calcium–aluminum-rich inclusions from CV chondrites, Geochim. Cosmochim. Acta 67 (2003) 3165–3179.
[60] K.K. Marhas, J.N. Goswami, Be–B isotope systematics in CV and CM hibonites: implications for solar energetic particle production of short-lived nuclides in early solar system, Lunar Planet. Sci. XXXIV (2003) (#1303 [CD-ROM]).
[61] T. Ushikubo, Y. Guan, L.A. Leshin, ^{10}Be–^{10}B systematics of hibonite-bearing inclusions from Murchison (CM2) and Kainsaz (CO3), Lunar Planet. Sci. XXXIV (2006) (#2368 [CD-ROM]).